



## Article

# Low-Rank Tensor Fusion for Enhanced Deep Learning-Based Multimodal Brain Age Estimation

Xia Liu <sup>1</sup>, Guowei Zheng <sup>2</sup>, Iman Beheshti <sup>3,\*</sup> , Shanling Ji <sup>4</sup>, Zhinan Gou <sup>1</sup> and Wenkuo Cui <sup>1</sup>

<sup>1</sup> School of Management Science and Information Engineering, Hebei University of Economics and Businesses, Shijiazhuang 050061, China; liux@hueb.edu.cn (X.L.); zhinan.gou@hotmail.com (Z.G.); wenkuo@tongji.edu.cn (W.C.)

<sup>2</sup> School of Computer Science and Technology, Harbin Institute of Technology, Weihai 264209, China; zhenggw@stu.hit.edu.cn

<sup>3</sup> Department of Human Anatomy and Cell Science, University of Manitoba, Winnipeg, MB R3T 2N2, Canada

<sup>4</sup> Institute of Mental Health, Jining Medical University, Jining 272111, China; jishanling@mail.jnmc.edu.cn

\* Correspondence: iman.beheshti@umanitoba.ca

**Abstract: Background/Objectives:** A multimodal brain age estimation model could provide enhanced insights into brain aging. However, effectively integrating multimodal neuroimaging data to enhance the accuracy of brain age estimation remains a challenging task. **Methods:** In this study, we developed an innovative data fusion technique employing a low-rank tensor fusion algorithm, tailored specifically for deep learning-based frameworks aimed at brain age estimation. Specifically, we utilized structural magnetic resonance imaging (sMRI), diffusion tensor imaging (DTI), and magnetoencephalography (MEG) to extract spatial-temporal brain features with different properties. These features were fused using the low-rank tensor algorithm and employed as predictors for estimating brain age. **Results:** Our prediction model achieved a desirable prediction accuracy on the independent test samples, demonstrating its robust performance. **Conclusions:** The results of our study suggest that the low-rank tensor fusion algorithm has the potential to effectively integrate multimodal data into deep learning frameworks for estimating brain age.



**Citation:** Liu, X.; Zheng, G.; Beheshti, I.; Ji, S.; Gou, Z.; Cui, W. Low-Rank Tensor Fusion for Enhanced Deep Learning-Based Multimodal Brain Age Estimation. *Brain Sci.* **2024**, *14*, 1252. <https://doi.org/10.3390/brainsci14121252>

Academic Editors: Kaundinya Gopinath and David Han

Received: 20 September 2024

Revised: 26 November 2024

Accepted: 10 December 2024

Published: 13 December 2024



**Copyright:** © 2024 by the authors. Licensee MDPI, Basel, Switzerland. This article is an open access article distributed under the terms and conditions of the Creative Commons Attribution (CC BY) license (<https://creativecommons.org/licenses/by/4.0/>).

**Keywords:** brain age; spatial-temporal; multimodal; low-rank tensor fusion; machine learning; deep learning

## 1. Introduction

Brain aging is the gradual decline of mental function. The “brain age” biomarker measures the aging status of the brain [1]. Advanced machine and deep learning techniques, combined with brain imaging scans, are used to derive brain age [2–7]. Studying brain aging can help identify markers that indicate its progression.

Functional magnetic resonance imaging (fMRI), structural magnetic resonance imaging (sMRI), diffusion tensor imaging (DTI), and magnetoencephalography (MEG) have been instrumental in detecting age-related changes in the brain [8–10]. Among these modalities, sMRI is commonly used to estimate brain age due to its high-resolution images that enable tracking of structural brain changes [10–12]. Moreover, sMRI data are more widely available than other modalities, enhancing the reproducibility of brain age research [13]. For instance, Cao et al. applied the least absolute shrinkage and selection operator (LASSO) algorithm to longitudinal sMRI data from 303 healthy controls (HCs) for predicting individual brain maturity [14]. Beheshti et al. introduced a unique 3D patch-based grading procedure for estimating cortical aging using sMRI data [15,16]. Franke et al. presented a framework for efficiently estimating the brain age of 650 HCs from their sMRI scans using a kernel method for regression [17]. Valizadeh et al. employed sMRI data from 3144 HCs to extract various anatomical features and using them to predict age through different statistical techniques [18]. Cole et al. used convolutional neural networks to estimate brain age

using raw sMRI data from 2001 HCs [19]. Lancaster et al. trained a Bayesian optimization framework with data from 2003 HCs to predict age [20]. Liu et al. constructed a multi-feature-based network (MFN) to estimate the brain age of 2501 HCs by describing structural similarities between traditional cortical morphological features [21]. Liem et al. assessed functional connectomes and mean time series from both cortical and subcortical regions, using support vector regression and regression based on random forest methodology to predict brain age [22]. Martina J. Lund employed resting-state fMRI data from 1126 HCs to estimate functional connectivity between brain networks, using these as features to predict brain age [23].

In addition to the aforementioned techniques, DTI enables the identification of diffusion and topological patterns across diverse brain regions, thereby aiding in the prediction of aging [24]. Benson Mwangi et al. applied a multivariate technique, relevance vector regression, to predict age using features extracted from diffusion tensor imaging [25].

Previous studies have primarily estimated brain age using single-modal neuroimaging data. Research has demonstrated that data fusion among data from various imaging methods could provide a more robust machine learning model and also provide a more comprehensive understanding of brain function, structure, and connectivity [26,27]. In the area of brain age estimation, recent research studies have also focused on integrating features from multiple modalities, demonstrating improved accuracy in brain age prediction [28–31]. For instance, D.A. Engemann et al. combined MRI, fMRI, and MEG features to estimate brain age [32].

It is well known that the T1 signal intensity of brain structures varies with age due to changes in brain tissue composition [33,34]. DTI helps to detect changes in diffusion and topological patterns in the brain associated with aging [24]. Thus, studies using unimodal features often fail to simultaneously account for age-related functional and structural changes in spatial and temporal domains, which could potentially improve prediction performance. Therefore, the combination of sMRI and diffusion images with functional metrics (such as EEG/MEG or fMRI) holds promise for enhancing brain age prediction. However, a key challenge in developing multimodal brain age estimation frameworks is the effective integration of data from diverse sources. This integration is crucial for improving prediction performance and providing a comprehensive view of structural and functional brain features throughout the brain aging process.

Recently, fusion techniques for brain age estimation have integrated information from neuroimaging modalities. Traditional methods like concatenation and early fusion may overlook modality specifics, leading to overfitting [35]. Middle fusion, like canonical correlation analysis (CCA), seeks common representations but may miss critical information [36]. Late fusion reduces overfitting but may limit performance by ignoring modality interactions [37]. Advanced deep learning, like autoencoders and variational autoencoders (VAEs), models complex interactions but faces generalizability challenges [38]. Tensor-based fusion captures higher-order relationships but is computationally demanding [39].

To overcome these challenges, our study introduces a low-rank tensor fusion approach. This approach employed low-rank tensors for multimodal fusion, enhancing the accuracy of brain age predictions by integrating structural and functional features. Specifically, we assessed the low-rank tensor fusion technique on both structural and functional brain features, comparing the effects of fused versus non-fused features within our brain age prediction model. Our findings demonstrated that our model performs comparably to state-of-the-art models across three multimodal tasks evaluated on public datasets.

## 2. Materials and Methods

### 2.1. Dataset and Data Availability

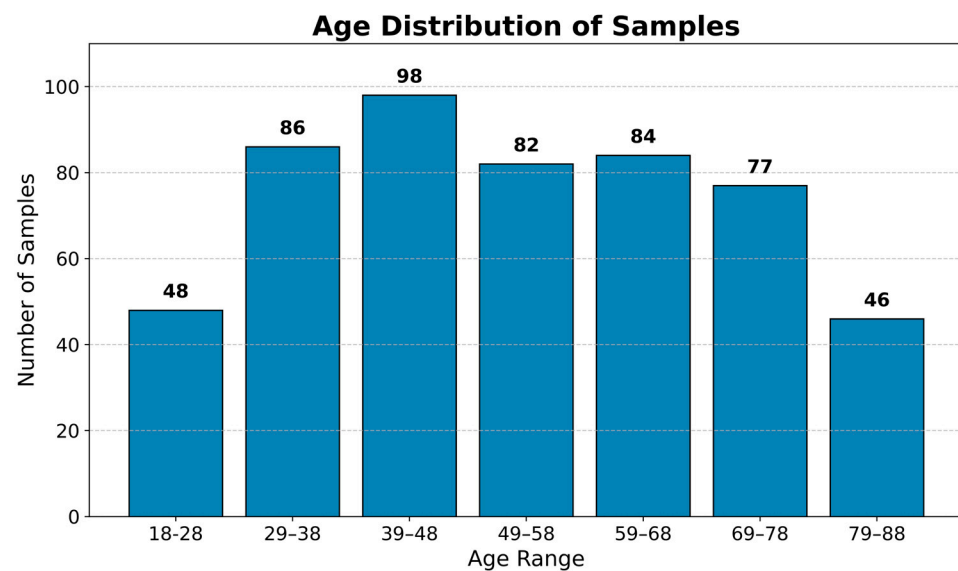
We used data from the Cambridge Center for Aging Neuroscience (Cam-CAN) [40,41]. Further details are available at <https://camcan-archive.mrc-cbu.cam.ac.uk//dataaccess/>; accessed on 15 February 2024. Table 1 summarizes the imaging parameters.

**Table 1.** The imaging parameters of different neuroimaging data used for brain age modeling.

Scans Type	Sequence	TR (ms)	TE (ms)	Flip Angle (°)	FOV (mm)	Voxel Size (mm)
sMRI	MPRAGE	2250	2.99	9	256 × 240 × 192	1 × 1 × 1
Diffusion-weighted		9100	104		192 × 192	2 × 2 × 2
Resting-state MEG	Sampling rate (HZ)	Duration (min:s)		Task		
	1000	08:40		Rest with eyes closed		

Abbreviations: sMRI, structural magnetic resonance imaging. TR, the Alzheimer’s Disease Neuroimaging Initiative. TE, Echo Time. MPRAGE, Magnetization Prepared-Rapid Gradient Echo imaging.

In this study, we utilized neuroimaging data from three modalities: sMRI, MEG, and DTI. A total of 521 HCs (270 males, 251 females, aged 18–88, mean age:  $52.3 \pm 17.7$ ) underwent MR imaging using a 3T scanner. Figure 1 illustrates the age distribution of the participants included in the study. Resting-state MEG data were acquired using a 306-channel system (102 magnetometers, 204 planar gradiometers) with a sampling rate of 1 kHz for 8 min and 40 s with eyes closed. The acquisition parameters were as follows: Flip angle =  $9^\circ$ , field of view =  $256 \times 240 \times 192 \text{ mm}^3$ , voxel size = 1 mm.

**Figure 1.** The age distribution of the participants.

## 2.2. Neuroimaging Data Processing

### 2.2.1. sMRI Data Preprocessing

sMRI images were preprocessed using SPM12 for affine registration, realignment, bias correction, and white matter (WM)/gray matter (GM)/cerebrospinal fluid (CSF) segmentation. CAT12 toolbox (Version 12.9; <https://neuro-jena.github.io/cat/index.html> accessed on 9 December 2024) was used for estimating WM and GM probability maps with default settings [42]. Skull stripping and registration to standard space were performed using the Montreal Neurological Institute (MNI) 152 template. Following tissue segmentation and bias correction, probability maps of WM, GM, and CSF [43] were generated.

### 2.2.2. MEG Data Preprocessing

The MEG data were preprocessed using temporal extension (tSSS) in Elekta NeuroMag MaxFilter v2.2 for independent head motion correction and noise reduction, with a correlation limit of 0.98 and a 10-s correlation window [44]. Subsequently, Brainstorm [45] was utilized for further MEG data processing, following the procedure described in Niso et al. [46]. High-pass and notch filters were applied at 0.3 Hz and 60 Hz and harmonics,

respectively. Cortical surface reconstruction from sMRI was performed using the recon-all algorithm in FreeSurfer (Version 6; <https://surfer.nmr.mgh.harvard.edu/> accessed on 9 December 2024) [47–49]. After the completion of source reconstruction, the computation of the power spectral density (PSD) was performed encompassing the entire duration of the resting-state scan.

### 2.2.3. Diffusion MRI Data Preprocessing

The diffusion MRI (dMRI) analyses were conducted using SPM12 with the aa 4.2 pipelines [50] and modules [51]. In the DTI stream, the data underwent skull-stripping using the Brain Extraction Tool (BET) utility in FMRIB’s Software Library (FSL; <https://fsl.fmrib.ox.ac.uk/fsl/docs/#/> accessed on 9 December 2024). Later, a parallel branch was employed to nonlinearly estimate the second-order diffusion tensor and its metrics (i.e., fractional anisotropy (FA), mean diffusion (MD), axial diffusion (AD), etc.).

## 2.3. Multimodal Fusion Model

### 2.3.1. Problem Modeling

As shown in Figure 2, we first extracted high-level abstract features for multiple modalities. For the extraction of DTI and sMRI features, in order to save computational resources and adapt to neuroimaging datasets with less data, we utilized two identical simple fully convolutional networks (SFCNs) [52] to obtain DTI and sMRI features. Each SFCN comprised six parts. The first five parts contained a 3D convolutional layer with  $3 \times 3 \times 3$  convolutional kernels (with channel numbers 32, 64, 128, 256, 256), followed by a batch normalization layer, a  $2 \times 2 \times 2$  maximum pooling layer, and was activated using the Rectified Linear Unit (ReLU) function. The sixth part consisted of a 3D convolutional layer with a  $1 \times 1 \times 1$  convolutional kernel size and 64 channels, a batch normalization layer, activated using the ReLU function, and finally, a  $3 \times 4 \times 3$  average pooling layer. To extract MEG features, we incorporated different attention values for each brain region using the Transformer Encoder [53]. Next, we employed two 1-dimensional convolutional layers with a convolutional kernel size of 1 and channel numbers of 128 and 32, respectively, as well as an average pooling layer to capture the local information from neighboring time points and summarize them [54,55]. Then, a fully connected layer with 64 neurons was used for dimensionality reduction to obtain the extracted MEG features. Finally, a layer with low-rank tensor fusion was added before the fully connected layer. Brain age was estimated from brain images of subjects by feature extraction, low-rank tensor fusion of multimodal features, and mapping with chronological age as label.

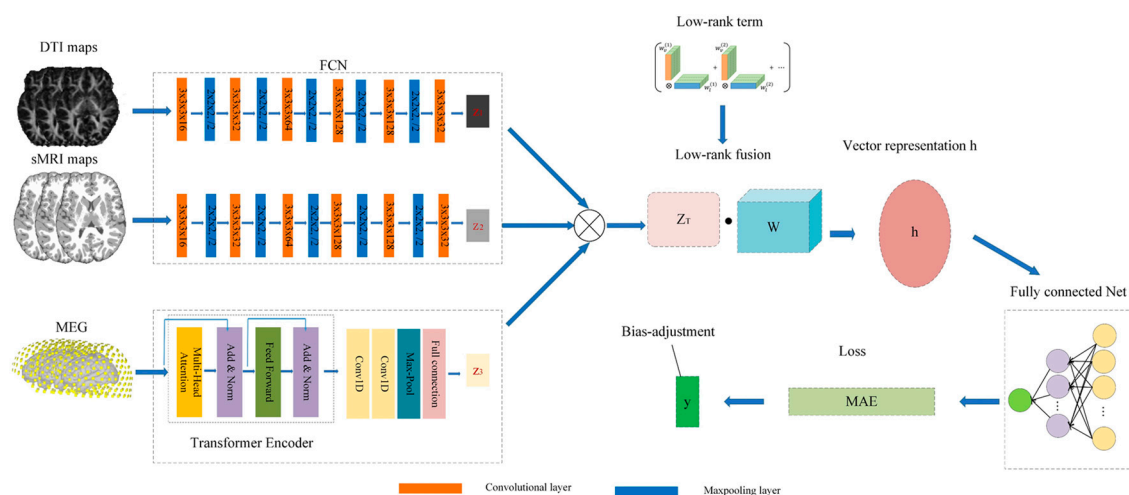


**Figure 2.** The overview of our proposed approach to fusing multimodal features to predict brain age.

### 2.3.2. Tensor Fusion and Representation

Tensor representation is a successful approach for multimodal fusion. Prior research has indicated that this method outperforms basic concatenation or pooling strategies in capturing multimodal interactions [56,57]. The tensor  $Z$  is computed by the following:

$$Z = \bigotimes_{m=1}^M z_m, z_m \in R^{d_m} \quad (1)$$

$M$  represents the total number of input modalities and  $z_i$  ( $i = 1, 2, 3, \dots, M$ ) represents the features extracted from the multimodal data. The tensor outer product is denoted by  $\bigotimes_{m=1}^M$ . The resulting feature after fusion is denoted by  $Z_T$ . The tensor  $Z$  is then fed into a linear layer  $g(\cdot)$ , which produces a vector representation as follows:

$$h = g(Z; \mathcal{W}, b) = \mathcal{W} \cdot Z + b \quad (2)$$

where  $\mathcal{W}$  is the weight of this layer and  $b$  is the bias. With  $Z$  being an order- $M$  tensor. In the tensor dot product  $\mathcal{W} \cdot Z$ , the weight  $\mathcal{W}$  can be partitioned into  $\tilde{\mathcal{W}}_k$ ,  $k = 1, \dots, d_m$ . Each  $\tilde{\mathcal{W}}_k$  contributes to one dimension in the output vector  $h$ , i.e.,  $h_k = \tilde{\mathcal{W}}_k \cdot Z$ .

The specific process is as Algorithm 1:

---

**Algorithm 1.** Multimodal low-rank tensor fusion algorithm.

---

Input: sMRI maps; DTI maps; MEG; label: chronologic age  $y$

Output: brain age  $\hat{y}$

Parameters: rank, drop rate  $\eta$

---

- 1: sMRI maps and DTI maps were processed using FCN to extract the spatial structure features  $z_1$  and  $z_2$
  - 2: The PSD extracted using MEG are passed through the Encoder of Transformer to extract brain temporal features  $z_3$
  - 3: Low-rank fusion  $Z_T$
  - 4: The fusion feature vector expressed as  $h = g(Z; \mathcal{W}, b) = \mathcal{W} \cdot Z + b$
  - 5: Access a fully connected network
  - 6: Minimize the loss function  $MAE$
  - 7: Output bias corrected values for brain age
- 

### 2.4. Model Implementation and Validation

To reduce the reliance on the disparity in brain age (brain age gap = predict brain age – chronological age) on age, a bias correction was applied [58]. To evaluate the model, we used  $R^2$ , root mean square error (RMSE), and MAE as metrics.

$$MAE = \frac{1}{n} \left( \sum_{i=1}^n |y_i - Y_i| \right) \quad (3)$$

$$RMSE = \sqrt{\frac{1}{n} \sum_{i=1}^n (y_i - Y_i)^2} \quad (4)$$

$$R^2 = 1 - \frac{\sum_{i=1}^n (y_i - Y_i)^2}{\sum_{i=1}^n (y_i - \bar{y})^2} \quad (5)$$

The model is implemented in Python 3.7 and Pytorch1.11.0 library and was executed on the Ubuntu 18.04 operating system. Throughout the training period, we utilized MAE as the loss function with the Adam optimizer [59] using a learning rate of  $1 \times 10^{-4}$  and weight decay of  $1 \times 10^{-8}$ . Additionally, we employed a mini-batch size of 12 and trained for a total of 300 epochs. When the model performs best on the validation set, we save it as the final model and use it for testing.

To evaluate the model, 521 subjects were randomly divided into training (416), validation (52), and testing (53) groups.

### 3. Results

#### 3.1. Estimation Based on Different Features and Fusion Methods

The results of different features and fusion methods on the dataset are presented in Table 2. In summary, our multimodal low-rank fusion method generally outperforms the unimodality. Specifically, we designed the low-rank fusion module to combine multimodal features, resulting in a lower *MAE* and higher  $R^2$ , while the competing unimodal-based methods achieved an optimal *MAE* of 4.54 and  $R^2 = 0.92$ , respectively. Our multimodal low-rank fusion model achieves smaller age errors compared to other non-fusion models.

**Table 2.** Performance metrics for various features and fusion methods.

	Strategies	Feature	MAE (y)	RMSE (y)	$R^2$	<i>p</i>
Training set	Unimodal	DTI	11.67	12.13	0.74	<0.001
		MEG	-	-	-	-
		sMRI	3.83	4.72	0.94	<0.001
	Traditional fusion	Add	2.89	4.30	0.96	<0.001
		Concat	3.11	4.43	0.96	<0.001
	Low-rank tensor fusion	sMRI + AD + PSD	2.30	2.94	0.96	<0.001
sMRI + MD + PSD		3.04	3.82	0.95	<0.001	
<b>sMRI + FA + PSD</b>		<b>2.25</b>	<b>2.85</b>	<b>0.98</b>	<0.001	
Validation set	Unimodal	DTI	12.69	14.56	0.71	<0.001
		MEG	-	-	-	-
		sMRI	4.91	5.61	0.91	<0.001
	Traditional fusion	Add	7.91	9.29	0.89	<0.001
		Concat	10.65	12.17	0.79	<0.001
	Low-rank tensor fusion	sMRI + AD + PSD	5.32	6.67	0.90	<0.001
sMRI + MD + PSD		4.80	6.18	0.90	<0.001	
<b>sMRI + FA + PSD</b>		<b>4.49</b>	<b>5.72</b>	<b>0.92</b>	<0.001	
Testing set	Unimodal	DTI	13.52	15.68	0.57	<0.001
		MEG	-	-	-	-
		sMRI	4.54	5.52	0.92	<0.001
	Traditional fusion	Add	8.56	10.13	0.90	<0.001
		Concat	11.36	13.46	0.72	<0.001
	Low-rank tensor fusion	sMRI + AD + PSD	4.59	5.90	0.91	<0.001
sMRI + MD + PSD		4.47	5.45	0.92	<0.001	
<b>sMRI + FA + PSD</b>		<b>4.20</b>	<b>5.43</b>	<b>0.93</b>	<0.001	

Abbreviations: *MAE*, mean absolute error. *RMSE*, root mean square error.  $R^2$ , the coefficient of determination. DTI, diffusion tensor imaging. MEG, magnetoencephalography. sMRI, structural magnetic resonance imaging. AD, axial diffusivity. MD, mean diffusivity. FA, fractional anisotropy. PSD, power spectral density. The symbol “-” indicates that this result is not reported. Add: a parallel strategy to combine the two feature vectors into a compound vector. Concat: a series of feature fusion methods, directly linking the features. The prediction results using MEG data are not reported because the depth prediction model did not converge.

We employ various combinations of multimodal features to predict brain age. As depicted in Table 2, the prediction model achieves optimal performance when fusing sMRI, FA, and PSD. The subsequent analyses are based on the prediction results from the fusion model that utilized the optimal feature combination. Moreover, we compared traditional feature fusion methods, such as addition or concatenation of these features, and found that our low-rank tensor fusion outperformed these traditional methods in predicting brain age.

### 3.2. Estimation Based on Low-Rank Tensor Fusion Method

In Table 2, the results demonstrate the effectiveness of our low-rank tensor fusion approach for age prediction. In the training set, we achieved an  $R^2$  value of 0.98, with a MAE of 2.25 years and RMSE of 2.85 years (refer to Figure 3A). This indicates the successful fusion of features in improving age prediction accuracy. Furthermore, on the validation set, our method yielded an MAE of 4.49 years,  $R^2$  of 0.92, and RMSE of 5.72 years (refer to Figure 3B). On the test set, we obtained an MAE of 4.20 years,  $R^2$  of 0.93, and RMSE of 5.43 years (refer to Figure 3C).

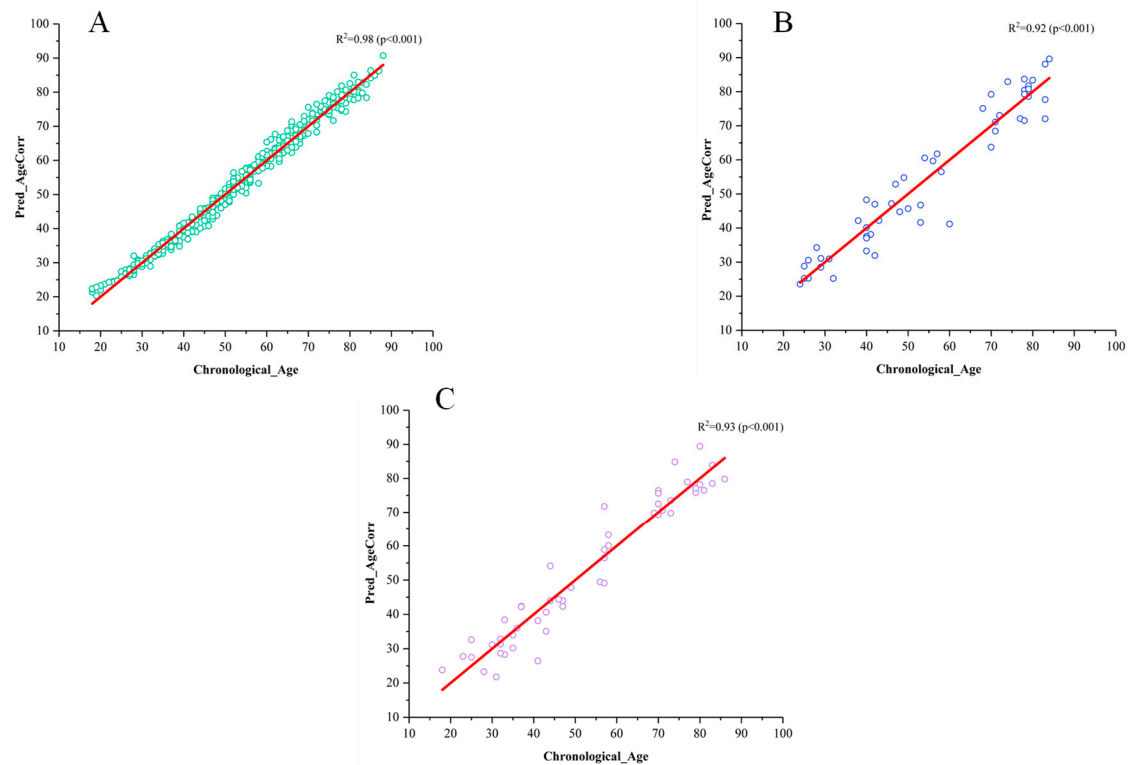


**Figure 3.** Model performance on each dataset. (A) Is the model performance on the training set. (B) Is the model performance on the validation set. (C) Is the model performance on the test set.

## 4. Discussion

Multimodal brain imaging data are extensively utilized for estimating brain age across various contexts. Niu et al. explored different analysis strategies for brain age prediction using large datasets encompassing sMRI, DTI, and fMRI data [60]. Similarly, De Lange et al. utilized machine learning and multimodal imaging data to predict brain age, encompassing gray matter, white matter, and resting-state functional connectivity [61]. Their findings highlighted improved prediction accuracy with the inclusion of multimodal features in the model. Rokicki et al. utilized T1 and T2 structural imaging data, along with cerebral blood flow data from arterial spin labeling, to develop a multimodal model for estimating brain age [62]. Their study demonstrated that integrating multiple types of data can enhance the accuracy of brain age prediction.

We aimed to test whether the use of multimodal neuroimaging data can improve the accuracy of predicting brain age and how to fuse features more effectively. As shown in Table 2, when single-mode features were used to predict brain age, sMRI performed better than either DTI or MEG data (MAE = 4.54 years, RMSE = 5.52 years,  $R^2 = 0.92$  based on structural data vs. MAE = 13.52 years, RMSE = 15.68 years,  $R^2 = 0.57$  based on DTI data). When predicting brain age based on MEG data, the depth prediction model did not converge, so the prediction results were not reported. As a result, multimodal data improved prediction performance, as we hypothesized. Specifically, when unimodal data

were used to predict brain age, sMRI performed best. This may be because sMRI can more easily capture brain anatomical changes and structural variations in the brain [11], which may better reflect aging [63–66]. Therefore, the majority of studies used sMRI data to estimate brain age [30,67].

Despite the macroscopic nature of morphological features derived from sMRI data, their sensitivity to neurodevelopmental microstructural changes is limited [68,69]. To enhance model predictive performance, integration of additional modalities is crucial. For example, diffusion MRI techniques, which are adept at capturing tissue microstructure by tracking water molecule diffusion and probing cellular-level environments, offer promising insights [70]. While numerous studies have effectively utilized DTI data to predict brain age, dMRI faces technical challenges and exhibits higher variability compared to conventional modalities like T1- and T2-weighted imaging [71,72]. These intricacies can introduce nonlinear distortions in the original images, affecting diffusion metrics like MD and FA [72], which can reduce the performance of the prediction model. This may also be one of the reasons why the MAE is larger when using DTI prediction alone. In the application of functional data, improvements in the prediction of brain age using fMRI are limited by the hysteresis of the hemodynamic response function [73]. However, the MEG with high spatial and temporal resolution can provide complementary features related to normal aging. In exploring MEG data for brain age estimation, we found that the prediction model failed to converge stably, highlighting common challenges in deep learning with complex feature sets, especially during extraction and training. In a previous study, PSD features combined with a machine learning regression model were used to predict brain age, and the MAE value was obtained [30]. This is something we need to consider improving in the future.

In this study, we use resting-state MEG (magnetoencephalography), which is preferred over task-based MEG for studying age-related brain changes because it captures the brain's spontaneous neural activity without the influence of external tasks [74]. This provides a clearer picture of the brain's intrinsic functional organization and baseline neural efficiency. Unlike task-based paradigms, which can introduce variability due to individual differences in task performance and cognitive strategies, resting-state MEG offers a more stable and reliable measure of brain connectivity, especially in key frequency bands like alpha and beta, which are sensitive to aging.

Compared to fMRI, resting-state MEG has several advantages. First, MEG offers high temporal resolution, capturing brain activity on the millisecond scale, while fMRI operates on a much slower, second-level timescale, potentially missing important rapid oscillatory patterns [75]. MEG also directly measures neuronal activity through magnetic fields, while fMRI relies on the slower BOLD signal, which is influenced by hemodynamic processes rather than direct neural firing [76]. Furthermore, MEG is less sensitive to motion artifacts, providing clearer data, especially for older adults who may have difficulty remaining still. These advantages make MEG particularly well-suited for detecting age-related functional changes in the brain [74].

During the feature extraction phase, we opted for the SFCNs technique to extract features from sMRI and DTI data due to its exceptional ability to capture both local and hierarchical spatial patterns necessary for analyzing brain structure. SFCNs can identify detailed patterns in both gray and white matter across different brain regions, which is crucial for detecting age-related changes. Unlike traditional CNNs, SFCNs preserve spatial resolution throughout the network, meaning they can extract fine-grained features without losing information during down sampling. This ability makes SFCNs particularly well-suited for working with sMRI and DTI data, where maintaining spatial accuracy is important. Research has shown that SFCNs outperform other methods, like traditional CNNs, in extracting structural features from brain imaging data [77].

When FCN and Transformer Encoder were used to process the data and then used to predict brain age after low-rank tensor fusion, the prediction performance of the model was significantly improved. Notably, the fusion of sMRI, FA, and PSD features achieved



the highest prediction ability. This is inseparable from the advantages of FCN. Moreover, the Transformer method was introduced by [53], which is mainly based on self-attention and has been applied to many tasks, such as natural language processing, classification tasks [78,79], and brain age prediction [80–83]. This is because the feature extraction capability of the Transformer method is superior to that of the Recurrent Neural Network, and the source and target sequences can be “self-associated” with each other. In this way, the information contained in the representation of the source and target sequences is richer, and subsequent layers of feed-forward networks improve the representation of the model. These advantages have enhanced the performance of our models.

Our fusion mechanism, which employs low-rank tensor fusion, allows us to utilize tensor rank minimization to learn tensors that more precisely capture the true correlations and underlying structures within multimodal data, effectively reducing input errors [84,85]. Studies have shown that FA is the most age-sensitive of the conventional DTI metrics [86]. This may be one of the reasons why our prediction model with FA performs better in feature fusion. In contrast to the conventional approach of fusing multiple modes of features, the MAE value is reduced, and the prediction result is more desirable. Table 3 summarizes the current studies using Cam-CAN data to predict brain age as well as our proposed method. Specifically, Xifra-Porxas, Alba, et al. [30] used dimensionality reduction techniques and Gaussian process regression (GPR) to predict brain age. Using MEG features ( $MAE = 9.60$  years) produced worse performance than using MRI features ( $MA = 5.33$  years), but a stacked model combining the two features improved age prediction performance ( $MAE = 4.88$  years). Popescu, Sebastian G et al. [87] have trained a U-Net model that utilizes deep learning techniques to generate individualized 3D brain maps at a local level for age prediction, which could provide spatial information about anatomical patterns of brain aging. The Cam-CAN data were then tested on the model and the MAE was 9.5 years. Han, Juhyuk et al. [88] trained and compared the predictive performance of 27 machine learning models for brain age prediction and applied the trained models to the Cam-CAN dataset. The MAE and  $R^2$  were 7.08–10.50 years and 0.64–0.85, respectively. A brain age prediction model was constructed by using the transfer learning method and a large dMRI dataset as the source domain. Then, the trained model was used to test Cam-CAN data, and the MAE was 4.68–5.71 years [89]. From Table 3, we can see that our proposed method has achieved a better performance than that of other previous studies.

**Table 3.** Comparative results of brain age estimation on Cam-CAN data.

Studies	Modal	MAE (y)	$R^2$
[30]	sMRI, MEG	4.88–9.6	-
[87]	sMRI	9	-
[88]	sMRI	7.08–10.50	0.64–0.85
[89]	dMRI	4.68–5.71	-
<b>Our method</b>	sMRI, MEG, DTI	<b>4.20</b>	<b>0.93</b>

Abbreviations: MAE, mean absolute error.  $R^2$ , the coefficient of determination. DTI, diffusion tensor imaging. MEG, magnetoencephalography. sMRI, structural magnetic resonance imaging. dMRI, diffusion magnetic resonance imaging.

Recently, with the broad application of multimodal data in brain age prediction, numerous advanced multimodal fusion methods have been proposed and have achieved promising results. For instance, Clements RG et al. leveraged a multimodal 3D convolutional neural network and magnetic resonance elastography (MRE) technology to predict brain age. The advantages of their method lie in the innovative combination of these two technologies, achieving high-precision brain age prediction, and further enhancing prediction accuracy through multimodal fusion, offering possibilities for the early diagnosis of neurodegenerative diseases. However, this method also has some drawbacks, including high model complexity, substantial computational resource requirements, strong data dependency, and limitations such as no performance improvement when incorporating damping ratio into the model [90]. The multimodal Transformer-based architecture

proposed by Wang J and his team demonstrates notable advantages in biological age prediction, including improved prediction accuracy through the fusion of facial, tongue, and retinal images, as well as its potential application in risk stratification and progression prediction of chronic diseases. However, this method also faces some challenges, such as the heterogeneity of the aging process limiting prediction accuracy, deployment difficulties due to technical complexity, and considerations regarding personal privacy and ethical issues [91].

Compared with these methods, our proposed low-rank tensor fusion approach demonstrates notable advantages in multimodal brain age prediction tasks. First, our method leverages low-rank tensor decomposition to effectively reduce redundant information within multimodal data, thus enhancing computational efficiency. Second, due to the automatic selection of salient features between modalities afforded by low-rank tensor decomposition, our method exhibits greater robustness under data imbalances [92]. Additionally, in terms of cross-dataset generalization, the low-rank tensor fusion method adapts better to feature differences across datasets, demonstrating high adaptability [93]. Additionally, by utilizing the low-rank tensor fusion technique, the likelihood of overfitting is minimized, while interpretability is enhanced through the extraction of crucial shared features instead of learning noise specific to each modality. This method has proven to be successful in various multimodal learning tasks, including the classification of neurodegenerative diseases [39], underscoring its resilience and efficacy.

In terms of potential clinical applications, our multimodal neuroimaging approach for brain age prediction holds promise in identifying individuals at risk of neurodegenerative diseases or monitoring disease progression. For instance, deviations between predicted and chronological brain age, known as brain age gaps, have been shown to serve as biomarkers for various neurological conditions, including dementia and other conditions [4,63]. By leveraging the improved prediction accuracy achieved through multimodal data integration, our model could potentially offer earlier and more accurate insights into brain health, facilitating timely interventions and personalized treatment strategies. We plan to explore these clinical implications in future studies.

Our study has several limitations. First, the sample size and the lack of an independent dataset for assessing the generalizability of our model are notable constraints. Our primary aim was to test the low-rank tensor fusion algorithm tailored for deep learning-based frameworks in brain age estimation. We used the Cambridge Center for Aging Neuroscience (Cam-CAN) dataset, which includes sMRI, DTI, and resting-state MEG data. While validating our results on an independent dataset could strengthen the findings, it is challenging to find a dataset that includes all three modalities, especially resting-state MEG data. Therefore, future studies should validate the proposed algorithm on larger, independent datasets. Another limitation involves the failure of our deep learning model to converge during training when using MEG data. This may have been due to issues such as improper weight initialization, inappropriate learning rates, insufficient data, overfitting, or a non-convex loss function. Despite adjusting factors like learning rate and weight initialization, the model did not converge using MEG data alone. However, the model did show convergence when combining MEG features with DTI and sMRI data. Future research with larger sample sizes is needed to investigate these convergence issues and propose solutions for deep learning models applied to brain imaging data. Additionally, in this study, we compared our low-rank tensor fusion algorithm with single-input data and traditional feature fusion methods, such as addition or concatenation. Our results demonstrated that the low-rank tensor fusion method provided better prediction accuracy than traditional feature fusion methods. Future studies could focus on developing more accurate deep learning-based data fusion methods and comparing them to existing techniques. It is important to note that the choice of data fusion method in deep learning models depends on factors such as data characteristics (e.g., structured, unstructured, multimodal), model complexity, and computational resources [94,95]. Finally, we intended to assess

our low-rank fusion method using combinations of all feature maps but were limited by computational resources. Future studies may be able to explore this approach further.

## 5. Conclusions

In this study, we presented a novel low-rank tensor fusion algorithm developed to integrate multimodal brain imaging data for the purpose of brain age estimation. Our strategy involves integrating three different imaging techniques—sMRI, DTI, and resting-state MEG—in order to offer a more thorough understanding of brain aging. We evaluated the method using the Cambridge Centre for Aging Neuroscience (Cam-CAN) dataset. The results indicated that incorporating both structural and functional brain features enables our model to offer a deeper understanding of the brain's aging process. Our data fusion method exhibited performance that rivals state-of-the-art techniques in different multimodal tasks, as tested on datasets that are publicly accessible.

**Author Contributions:** Conceptualization, X.L., I.B., W.C. and G.Z.; methodology, G.Z. and S.J.; software, X.L., G.Z., S.J., Z.G. and W.C.; validation, S.J. and W.C.; formal analysis, X.L.; data curation, X.L., G.Z., S.J. and Z.G.; writing—review and editing, I.B.; supervision, I.B.; funding acquisition, Z.G. and W.C. All authors have read and agreed to the published version of the manuscript.

**Funding:** This research was partially funded by the Science Research Project of the Hebei Education Department (Grant No. BJK2024092), the Hebei Natural Science Foundation (Grant No. F2023207003), and the Scientific Research and Development Program of Hebei University of Economics and Business (2024YB23).

**Institutional Review Board Statement:** This study utilized a publicly available dataset, which does not require IRB approval.

**Informed Consent Statement:** Written informed consent was obtained from all participants who attended The Cambridge Centre for Ageing and Neuroscience (Cam-CAN) study.

**Data Availability Statement:** We used data from the Cambridge Center for Aging Neuroscience (Cam-CAN): <https://camcan-archive.mrc-cbu.cam.ac.uk//dataaccess/> (15 February 2024).

**Acknowledgments:** This work was supported in part by the Science Research Project of Hebei Education Department (Grant No. BJK2024092), in part by Hebei Natural Science Foundation (Grant No. F2023207003), in part by Hebei University of Economics and Business Scientific Research and Development Program (2024YB23).

**Conflicts of Interest:** We declare that there are no conflicts of interest regarding the publication of this paper, and the manuscript is approved by all authors for publication.

## References

1. Cullen, N.C.; Mälärstig, A.; Stomrud, E.; Hansson, O.; Mattsson-Carlgrén, N. Accelerated inflammatory aging in Alzheimer's disease and its relation to amyloid, tau, and cognition. *Sci. Rep.* **2021**, *11*, 1965. [[CrossRef](#)]
2. Cole, J.H.; Franke, K. Predicting age using neuroimaging: Innovative brain ageing biomarkers. *Trends Neurosci.* **2017**, *40*, 681–690. [[CrossRef](#)] [[PubMed](#)]
3. Ballester, P.L.; da Silva, L.T.; Marcon, M.; Esper, N.B.; Frey, B.N.; Buchweitz, A.; Meneguzzi, F. Predicting Brain Age at Slice Level: Convolutional Neural Networks and Consequences for Interpretability. *Front. Psychiatry* **2021**, *12*. [[CrossRef](#)] [[PubMed](#)]
4. Franke, K.; Luders, E.; May, A.; Wilke, M.; Gaser, C. Brain maturation: Predicting individual BrainAGE in children and adolescents using structural MRI. *Neuroimage* **2012**, *63*, 1305–1312. [[CrossRef](#)] [[PubMed](#)]
5. Su, L.; Wang, L.; Shen, H.; Hu, D. Age-related classification and prediction based on MRI: A sparse representation method. *Procedia Environ. Sci.* **2011**, *8*, 645–652. [[CrossRef](#)]
6. Baecker, L.; Dafflon, J.; Da Costa, P.F.; Garcia-Dias, R.; Vieira, S.; Scarpazza, C.; Calhoun, V.D.; Sato, J.R.; Mechelli, A.; Pinaya, W.H. Brain age prediction: A comparison between machine learning models using region- and voxel-based morphometric data. *Hum. Brain Mapp.* **2021**, *42*, 2332–2346. [[CrossRef](#)]
7. Mishra, S.; Beheshti, I.; Khanna, P. A Review of Neuroimaging-driven Brain Age Estimation for identification of Brain Disorders and Health Conditions. *IEEE Rev. Biomed. Eng.* **2021**, *16*, 371–385. [[CrossRef](#)] [[PubMed](#)]
8. Matsuda, H.; Mizumura, S.; Nemoto, K.; Yamashita, F.; Imabayashi, E.; Sato, N.; Asada, T. Automatic voxel-based morphometry of structural MRI by SPM8 plus diffeomorphic anatomic registration through exponentiated lie algebra improves the diagnosis of probable Alzheimer Disease. *Am. J. Neuroradiol.* **2012**, *33*, 1109–1114. [[CrossRef](#)] [[PubMed](#)]

9. Franke, K.; Clarke, G.D.; Dahnke, R.; Gaser, C.; Kuo, A.H.; Li, C.; Schwab, M.; Nathanielsz, P.W. Premature brain aging in baboons resulting from moderate fetal undernutrition. *Front. Aging Neurosci.* **2017**, *9*, 92. [[CrossRef](#)] [[PubMed](#)]
10. Farokhian, F.; Yang, C.; Beheshti, I.; Matsuda, H.; Wu, S. Age-Related Gray and White Matter Changes in Normal Adult Brains. *Aging Dis* **2017**, *8*, 899–909. [[CrossRef](#)] [[PubMed](#)]
11. Matsuda, H. Voxel-based morphometry of brain MRI in normal aging and Alzheimer’s disease. *Aging Dis.* **2013**, *4*, 29. [[PubMed](#)]
12. Madan, C.R.; Kensinger, E.A. Cortical complexity as a measure of age-related brain atrophy. *NeuroImage* **2016**, *134*, 617–629. [[CrossRef](#)] [[PubMed](#)]
13. Sone, D.; Beheshti, I. Neuroimaging-based brain age estimation: A promising personalized biomarker in neuropsychiatry. *J. Pers. Med.* **2022**, *12*, 1850. [[CrossRef](#)]
14. Cao, B.; Mwangi, B.; Hasan, K.M.; Selvaraj, S.; Zeni, C.P.; Zunta-Soares, G.B.; Soares, J.C. Development and validation of a brain maturation index using longitudinal neuroanatomical scans. *Neuroimage* **2015**, *117*, 311–318. [[CrossRef](#)]
15. Beheshti, I.; Gravel, P.; Potvin, O.; Dieumegarde, L.; Duchesne, S. A novel patch-based procedure for estimating brain age across adulthood. *Neuroimage* **2019**, *197*, 618–624. [[CrossRef](#)] [[PubMed](#)]
16. Beheshti, I.; Potvin, O.; Duchesne, S. Patch-wise brain age longitudinal reliability. *Hum. Brain Mapp.* **2021**, *42*, 690–698. [[CrossRef](#)]
17. Franke, K.; Ziegler, G.; Klöppel, S.; Gaser, C.; Alzheimer’s Disease Neuroimaging Initiative. Estimating the age of healthy subjects from T1-weighted MRI scans using kernel methods: Exploring the influence of various parameters. *Neuroimage* **2010**, *50*, 883–892. [[CrossRef](#)] [[PubMed](#)]
18. Valizadeh, S.; Hänggi, J.; Méritat, S.; Jäncke, L. Age prediction on the basis of brain anatomical measures. *Hum. Brain Mapp.* **2017**, *38*, 997–1008. [[CrossRef](#)] [[PubMed](#)]
19. Cole, J.H.; Poudel, R.P.; Tsagkrasoulis, D.; Caan, M.W.; Steves, C.; Spector, T.D.; Montana, G. Predicting brain age with deep learning from raw imaging data results in a reliable and heritable biomarker. *NeuroImage* **2017**, *163*, 115–124. [[CrossRef](#)] [[PubMed](#)]
20. Lancaster, J.; Lorenz, R.; Leech, R.; Cole, J.H. Bayesian optimization for neuroimaging pre-processing in brain age classification and prediction. *Front. Aging Neurosci.* **2018**, *10*, 28. [[CrossRef](#)]
21. Liu, X.; Beheshti, I.; Zheng, W.; Li, Y.; Li, S.; Zhao, Z.; Yao, Z.; Hu, B. Brain age estimation using multi-feature-based networks. *Comput. Biol. Med.* **2022**, *143*, 105285. [[CrossRef](#)] [[PubMed](#)]
22. Liem, F.; Varoquaux, G.; Kynast, J.; Beyer, F.; Masouleh, S.K.; Huntenburg, J.M.; Lampe, L.; Rahim, M.; Abraham, A.; Craddock, R.C. Predicting brain-age from multimodal imaging data captures cognitive impairment. *Neuroimage* **2017**, *148*, 179–188. [[CrossRef](#)] [[PubMed](#)]
23. Lund, M.J.; Alnæs, D.; de Lange, A.-M.G.; Andreassen, O.A.; Westlye, L.T.; Kaufmann, T. Brain age prediction using fMRI network coupling in youths and associations with psychiatric symptoms. *NeuroImage Clin.* **2022**, *33*, 102921. [[CrossRef](#)] [[PubMed](#)]
24. Le Bihan, D.; Mangin, J.F.; Poupon, C.; Clark, C.A.; Pappata, S.; Molko, N.; Chabriat, H. Diffusion tensor imaging: Concepts and applications. *J. Magn. Reson. Imaging Off. J. Int. Soc. Magn. Reson. Med.* **2001**, *13*, 534–546. [[CrossRef](#)]
25. Mwangi, B.; Hasan, K.M.; Soares, J.C. Prediction of individual subject’s age across the human lifespan using diffusion tensor imaging: A machine learning approach. *Neuroimage* **2013**, *75*, 58–67. [[CrossRef](#)]
26. Cole, J.H. Multimodality neuroimaging brain-age in UK biobank: Relationship to biomedical, lifestyle, and cognitive factors. *Neurobiol. Aging* **2020**, *92*, 34–42. [[CrossRef](#)]
27. Li, L.; Wang, Y.; Zeng, Y.; Hou, S.; Huang, G.; Zhang, L.; Yan, N.; Ren, L.; Zhang, Z. Multimodal Neuroimaging Predictors of Learning Performance of Sensorimotor Rhythm Up-Regulation Neurofeedback. *Front. Neurosci.* **2021**, *15*, 699999. [[CrossRef](#)]
28. Irimia, A.; Torgerson, C.M.; Goh, S.-Y.M.; Van Horn, J.D. Statistical estimation of physiological brain age as a descriptor of senescence rate during adulthood. *Brain Imaging Behav.* **2015**, *9*, 678–689. [[CrossRef](#)] [[PubMed](#)]
29. Lin, L.; Jin, C.; Fu, Z.; Zhang, B.; Bin, G.; Wu, S. Predicting healthy older adult’s brain age based on structural connectivity networks using artificial neural networks. *Comput. Methods Programs Biomed.* **2016**, *125*, 8–17. [[CrossRef](#)] [[PubMed](#)]
30. Xifra-Porxas, A.; Ghosh, A.; Mitsis, G.D.; Boudrias, M.-H. Estimating brain age from structural MRI and MEG data: Insights from dimensionality reduction techniques. *NeuroImage* **2021**, *231*, 117822. [[CrossRef](#)]
31. Beheshti, I.; Maikusa, N.; Matsuda, H. The accuracy of T1-weighted voxel-wise and region-wise metrics for brain age estimation. *Comput. Methods Programs Biomed.* **2022**, *214*, 106585. [[CrossRef](#)] [[PubMed](#)]
32. Engemann, D.A.; Kozynets, O.; Sabbagh, D.; Lemaître, G.; Varoquaux, G.; Liem, F.; Gramfort, A. Combining magnetoencephalography with magnetic resonance imaging enhances learning of surrogate-biomarkers. *Elife* **2020**, *9*, e54055. [[CrossRef](#)]
33. Cho, S.; Jones, D.; Reddick, W.E.; Ogg, R.J.; Steen, R.G. Establishing norms for age-related changes in proton T1 of human brain tissue in vivo. *Magn. Reson. Imaging* **1997**, *15*, 1133–1143. [[CrossRef](#)] [[PubMed](#)]
34. Salat, D.H.; Lee, S.Y.; Van der Kouwe, A.; Greve, D.N.; Fischl, B.; Rosas, H.D. Age-associated alterations in cortical gray and white matter signal intensity and gray to white matter contrast. *Neuroimage* **2009**, *48*, 21–28. [[CrossRef](#)]
35. Liu, M.; Cheng, D.; Wang, K.; Wang, Y. Multi-Modality Cascaded Convolutional Neural Networks for Alzheimer’s Disease Diagnosis. *Neuroinformatics* **2018**, *16*, 295–308. [[CrossRef](#)]
36. Hardoon, D.R.; Szedmak, S.; Shawe-Taylor, J. Canonical correlation analysis: An overview with application to learning methods. *Neural. Comput.* **2004**, *16*, 2639–2664. [[CrossRef](#)]
37. Sui, J.; Adali, T.; Yu, Q.; Chen, J.; Calhoun, V.D. A review of multivariate methods for multimodal fusion of brain imaging data. *J. Neurosci. Methods* **2012**, *204*, 68–81. [[CrossRef](#)] [[PubMed](#)]

38. Martinez-Murcia, F.J.; Arco, J.E.; Jimenez-Mesa, C.; Segovia, F.; Illan, I.A.; Ramirez, J.; Gorris, J.M. Bridging Imaging and Clinical Scores in Parkinson's Progression via Multimodal Self-Supervised Deep Learning. *Int. J. Neural. Syst.* **2024**, *34*, 2450043. [[CrossRef](#)] [[PubMed](#)]
39. Miao, X.; Zhang, X.; Zhang, H. Low-rank tensor fusion and self-supervised multi-task multimodal sentiment analysis. *Multimed Tools Appl.* **2024**, *83*, 63291–63308. [[CrossRef](#)]
40. Shafto, M.A.; Tyler, L.K.; Dixon, M.; Taylor, J.R.; Rowe, J.B.; Cusack, R.; Calder, A.J.; Marslen-Wilson, W.D.; Duncan, J.; Dalgleish, T. The Cambridge Centre for Ageing and Neuroscience (Cam-CAN) study protocol: A cross-sectional, lifespan, multidisciplinary examination of healthy cognitive ageing. *BMC Neurol.* **2014**, *14*, 1–25. [[CrossRef](#)]
41. Taylor, J.R.; Williams, N.; Cusack, R.; Auer, T.; Shafto, M.A.; Dixon, M.; Tyler, L.K.; Henson, R.N. The Cambridge Centre for Ageing and Neuroscience (Cam-CAN) data repository: Structural and functional MRI, MEG, and cognitive data from a cross-sectional adult lifespan sample. *Neuroimage* **2017**, *144*, 262–269. [[CrossRef](#)] [[PubMed](#)]
42. Farokhian, F.; Beheshti, I.; Sone, D.; Matsuda, H. Comparing CAT12 and VBM8 for Detecting Brain Morphological Abnormalities in Temporal Lobe Epilepsy. *Front. Neurol.* **2017**, *8*, 428. [[CrossRef](#)]
43. Ashburner, J.; Friston, K.J. Unified segmentation. *Neuroimage* **2005**, *26*, 839–851. [[CrossRef](#)]
44. Taulu, S.; Simola, J. Spatiotemporal signal space separation method for rejecting nearby interference in MEG measurements. *Phys. Med. Biol.* **2006**, *51*, 1759. [[CrossRef](#)]
45. Tadel, F.; Bock, E.; Niso, G.; Mosher, J.C.; Cousineau, M.; Pantazis, D.; Leahy, R.M.; Baillet, S. MEG/EEG group analysis with brainstorm. *Front. Neurosci.* **2019**, *13*, 76. [[CrossRef](#)]
46. Niso, G.; Tadel, F.; Bock, E.; Cousineau, M.; Santos, A.; Baillet, S. Brainstorm pipeline analysis of resting-state data from the open MEG archive. *Front. Neurosci.* **2019**, *13*, 284. [[CrossRef](#)]
47. Dale, A.M.; Fischl, B.; Sereno, M.I. Cortical surface-based analysis: I. Segmentation and surface reconstruction. *Neuroimage* **1999**, *9*, 179–194. [[CrossRef](#)] [[PubMed](#)]
48. Fischl, B.; Van Der Kouwe, A.; Destrieux, C.; Halgren, E.; Ségonne, F.; Salat, D.H.; Busa, E.; Seidman, L.J.; Goldstein, J.; Kennedy, D. Automatically parcellating the human cerebral cortex. *Cereb. Cortex* **2004**, *14*, 11–22. [[CrossRef](#)]
49. Fischl, B.; Salat, D.H.; Busa, E.; Albert, M.; Dieterich, M.; Haselgrove, C.; Van Der Kouwe, A.; Killiany, R.; Kennedy, D.; Klaveness, S. Whole brain segmentation: Automated labeling of neuroanatomical structures in the human brain. *Neuron* **2002**, *33*, 341–355. [[CrossRef](#)] [[PubMed](#)]
50. Cusack, R.; Vicente-Grabovetsky, A.; Mitchell, D.J.; Wild, C.J.; Auer, T.; Linke, A.C.; Peelle, J.E. Automatic analysis (aa): Efficient neuroimaging workflows and parallel processing using Matlab and XML. *Front. Neuroinformatics* **2015**, *8*, 90. [[CrossRef](#)] [[PubMed](#)]
51. Smith, S.M.; Jenkinson, M.; Woolrich, M.W.; Beckmann, C.F.; Behrens, T.E.; Johansen-Berg, H.; Bannister, P.R.; De Luca, M.; Drobnjak, I.; Flitney, D.E. Advances in functional and structural MR image analysis and implementation as FSL. *Neuroimage* **2004**, *23*, S208–S219. [[CrossRef](#)] [[PubMed](#)]
52. Peng, H.; Gong, W.; Beckmann, C.F.; Vedaldi, A.; Smith, S.M. Accurate brain age prediction with lightweight deep neural networks. *Med. Image Anal.* **2021**, *68*, 101871. [[CrossRef](#)] [[PubMed](#)]
53. Vaswani, A.; Shazeer, N.; Parmar, N.; Uszkoreit, J.; Jones, L.; Gomez, A.N.; Kaiser, Ł.; Polosukhin, I. Attention is all you need. *Adv. Neural Inf. Process. Syst.* **2017**, *30*. Available online: [https://papers.nips.cc/paper\\_files/paper/2017/hash/3f5ee243547dee91fdb053c1c4a845aa-Abstract.html](https://papers.nips.cc/paper_files/paper/2017/hash/3f5ee243547dee91fdb053c1c4a845aa-Abstract.html) (accessed on 9 December 2024).
54. Roy, S.; Kiral-Kornek, I.; Harrer, S. ChronoNet: A deep recurrent neural network for abnormal EEG identification. In Proceedings of the Conference on Artificial Intelligence in Medicine in Europe, Poznan, Poland, 26–29 June 2019; pp. 47–56.
55. Yan, W.; Calhoun, V.; Song, M.; Cui, Y.; Yan, H.; Liu, S.; Fan, L.; Zuo, N.; Yang, Z.; Xu, K. Discriminating schizophrenia using recurrent neural network applied on time courses of multi-site fMRI data. *EBioMedicine* **2019**, *47*, 543–552. [[CrossRef](#)] [[PubMed](#)]
56. Zadeh, A.; Chen, M.; Poria, S.; Cambria, E.; Morency, L.-P. Tensor fusion network for multimodal sentiment analysis. *arXiv* **2017**, arXiv:1707.07250.
57. Fukui, A.; Park, D.H.; Yang, D.; Rohrbach, A.; Darrell, T.; Rohrbach, M. Multimodal compact bilinear pooling for visual question answering and visual grounding. *arXiv* **2016**, arXiv:1606.01847.
58. Beheshti, I.; Nugent, S.; Potvin, O.; Duchesne, S. Bias-adjustment in neuroimaging-based brain age frameworks: A robust scheme. *NeuroImage* **2019**, *24*, 102063. [[CrossRef](#)] [[PubMed](#)]
59. Kingma, D.P.; Ba, J. Adam: A method for stochastic optimization. *arXiv* **2014**, arXiv:1412.6980.
60. Niu, X.; Zhang, F.; Kounios, J.; Liang, H. Improved prediction of brain age using multimodal neuroimaging data. *Hum. Brain Mapp.* **2020**, *41*, 1626–1643. [[CrossRef](#)]
61. De Lange, A.-M.G.; Anatórk, M.; Suri, S.; Kaufmann, T.; Cole, J.H.; Griffanti, L.; Zsoldos, E.; Jensen, D.E.; Filippini, N.; Singh-Manoux, A. Multimodal brain-age prediction and cardiovascular risk: The Whitehall II MRI sub-study. *NeuroImage* **2020**, *222*, 117292. [[CrossRef](#)] [[PubMed](#)]
62. Rokicki, J.; Wolfers, T.; Nordhøy, W.; Tesli, N.; Quintana, D.S.; Alnæs, D.; Richard, G.; de Lange, A.M.G.; Lund, M.J.; Nørdbom, L. Multimodal imaging improves brain age prediction and reveals distinct abnormalities in patients with psychiatric and neurological disorders. *Hum. Brain Mapp.* **2021**, *42*, 1714–1726. [[CrossRef](#)]
63. Cole, J.H.; Leech, R.; Sharp, D.J.; Alzheimer's Disease Neuroimaging Initiative. Prediction of brain age suggests accelerated atrophy after traumatic brain injury. *Ann. Neurol.* **2015**, *77*, 571–581. [[CrossRef](#)] [[PubMed](#)]

64. Cole, J.H.; Annus, T.; Wilson, L.R.; Remtulla, R.; Hong, Y.T.; Fryer, T.D.; Acosta-Cabronero, J.; Cardenas-Blanco, A.; Smith, R.; Menon, D.K. Brain-predicted age in Down syndrome is associated with beta amyloid deposition and cognitive decline. *Neurobiol. Aging* **2017**, *56*, 41–49. [[CrossRef](#)] [[PubMed](#)]
65. Pardoe, H.R.; Cole, J.H.; Blackmon, K.; Thesen, T.; Kuzniecky, R.; Human Epilepsy Project Investigators. Structural brain changes in medically refractory focal epilepsy resemble premature brain aging. *Epilepsy Res.* **2017**, *133*, 28–32. [[CrossRef](#)] [[PubMed](#)]
66. Kaufmann, T.; van der Meer, D.; Doan, N.T.; Schwarz, E.; Lund, M.J.; Agartz, I.; Alnæs, D.; Barch, D.M.; Baur-Streubel, R.; Bertolino, A. Common brain disorders are associated with heritable patterns of apparent aging of the brain. *Nat. Neurosci.* **2019**, *22*, 1617–1623. [[CrossRef](#)]
67. Beheshti, I. Cocaine destroys gray matter brain cells and accelerates brain aging. *Biology* **2023**, *12*, 752. [[CrossRef](#)]
68. Deipolyi, A.R.; Mukherjee, P.; Gill, K.; Henry, R.G.; Partridge, S.C.; Veeraraghavan, S.; Jin, H.; Lu, Y.; Miller, S.P.; Ferriero, D.M. Comparing microstructural and macrostructural development of the cerebral cortex in premature newborns: Diffusion tensor imaging versus cortical gyration. *Neuroimage* **2005**, *27*, 579–586. [[CrossRef](#)]
69. Weston, P.S.; Simpson, I.J.; Ryan, N.S.; Ourselin, S.; Fox, N.C. Diffusion imaging changes in grey matter in Alzheimer’s disease: A potential marker of early neurodegeneration. *Alzheimer’s Res. Ther.* **2015**, *7*, 1–8. [[CrossRef](#)] [[PubMed](#)]
70. Kincses, Z.T.; Vécsei, L. Is diffusion magnetic resonance imaging the future biomarker to measure therapeutic efficacy in multiple sclerosis? *Eur. J. Neurol.* **2018**, *25*, 707–708. [[CrossRef](#)]
71. Malyarenko, D.I.; Newitt, D.; Wilmes, L.J.; Tudorica, A.; Helmer, K.G.; Arlinghaus, L.R.; Jacobs, M.A.; Jajamovich, G.; Taouli, B.; Yankeelov, T.E. Demonstration of nonlinearity bias in the measurement of the apparent diffusion coefficient in multicenter trials. *Magn. Reson. Med.* **2016**, *75*, 1312–1323. [[CrossRef](#)] [[PubMed](#)]
72. Mirzaalian, H.; Pierrefeu, A.d.; Savadjiev, P.; Pasternak, O.; Bouix, S.; Kubicki, M.; Westin, C.-F.; Shenton, M.E.; Rathi, Y. Harmonizing diffusion MRI data across multiple sites and scanners. In Proceedings of the International Conference on Medical Image Computing and Computer-Assisted Intervention, Munich, Germany, 5–9 October 2015; pp. 12–19.
73. Smith, S.M.; Miller, K.L.; Salimi-Khorshidi, G.; Webster, M.; Beckmann, C.F.; Nichols, T.E.; Ramsey, J.D.; Woolrich, M.W. Network modelling methods for FMRI. *Neuroimage* **2011**, *54*, 875–891. [[CrossRef](#)] [[PubMed](#)]
74. Schoonhoven, D.N.; Briels, C.T.; Hillebrand, A.; Scheltens, P.; Stam, C.J.; Gouw, A.A. Sensitive and reproducible MEG resting-state metrics of functional connectivity in Alzheimer’s disease. *Alzheimers Res. Ther.* **2022**, *14*, 38. [[CrossRef](#)]
75. Zhang, X.; Lei, X.; Wu, T.; Jiang, T. A review of EEG and MEG for brainnetome research. *Cogn Neurodyn.* **2014**, *8*, 87–98. [[CrossRef](#)]
76. Baillet, S. Magnetoencephalography for brain electrophysiology and imaging. *Nat. Neurosci.* **2017**, *20*, 327–339. [[CrossRef](#)]
77. Hosseini-Asl, E.; Gimel’farb, G.; El-Baz, A. Alzheimer’s disease diagnostics by a 3D deeply supervised adaptable convolutional network. *Front. Biosci. (Landmark Ed.)* **2018**, *23*, 584–596.
78. Li, C.; Cui, Y.; Luo, N.; Liu, Y.; Bourgeat, P.; Frripp, J.; Jiang, T. Trans-ResNet: Integrating Transformers and CNNs for Alzheimer’s disease classification. In Proceedings of the 2022 IEEE 19th International Symposium on Biomedical Imaging (ISBI), Kolkata, India, 28–31 March 2022; pp. 1–5.
79. Zheng, G.; Zhang, Y.; Zhao, Z.; Wang, Y.; Liu, X.; Shang, Y.; Cong, Z.; Dimitriadis, S.I.; Yao, Z.; Hu, B. A transformer-based multi-features fusion model for prediction of conversion in mild cognitive impairment. *Methods* **2022**, *204*, 241–248. [[CrossRef](#)]
80. Cai, H.; Gao, Y.; Liu, M. Graph Transformer Geometric Learning of Brain Networks Using Multimodal MR Images for Brain Age Estimation. *IEEE Trans. Med. Imaging* **2022**, *42*, 456–466. [[CrossRef](#)] [[PubMed](#)]
81. Dahan, S.; Xu, H.; Williams, L.Z.; Fawaz, A.; Yang, C.; Coalson, T.S.; Williams, M.C.; Newby, D.E.; Edwards, A.D.; Glasser, M.F. Surface Vision Transformers: Flexible Attention-Based Modelling of Biomedical Surfaces. *arXiv* **2022**, arXiv:2204.03408.
82. Dahan, S.; Williams, L.Z.; Fawaz, A.; Rueckert, D.; Robinson, E.C. Surface Analysis with Vision Transformers. *arXiv* **2022**. [[CrossRef](#)]
83. Yang, Y.; Guo, X.; Chang, Z.; Ye, C.; Xiang, Y.; Lv, H.; Ma, T. Estimating Brain Age with Global and Local Dependencies. In Proceedings of the IEEE International Conference on Image Processing (ICIP), Bordeaux, France, 16–19 October 2022.
84. Liang, P.P.; Liu, Z.; Tsai, Y.-H.H.; Zhao, Q.; Salakhutdinov, R.; Morency, L.-P. Learning representations from imperfect time series data via tensor rank regularization. *arXiv* **2019**, arXiv:1907.01011.
85. Shen, X.; Huang, J.; Sun, Y.; Li, M.; Pan, B.; Ding, W. Parallel Pathway Convolutional Neural Network with Low-rank Fusion for Brain Age Prediction. In Proceedings of the 2021 IEEE 1st International Conference on Digital Twins and Parallel Intelligence (DTPI), Beijing, China, 15 July–15 August 2021; pp. 434–437.
86. Beck, D.; de Lange, A.-M.G.; Maximov, I.I.; Richard, G.; Andreassen, O.A.; Nordvik, J.E.; Westlye, L.T. White matter microstructure across the adult lifespan: A mixed longitudinal and cross-sectional study using advanced diffusion models and brain-age prediction. *NeuroImage* **2021**, *224*, 117441. [[CrossRef](#)] [[PubMed](#)]
87. Popescu, S.G.; Glocker, B.; Sharp, D.J.; Cole, J.H. Local brain-age: A U-net model. *Front. Aging Neurosci.* **2021**, *13*, 761954. [[CrossRef](#)] [[PubMed](#)]
88. Han, J.; Kim, S.Y.; Lee, J.; Lee, W.H.J.S. Brain Age Prediction: A Comparison between Machine Learning Models Using Brain Morphometric Data. *Hum. Brain Mapp.* **2022**, *22*, 8077. [[CrossRef](#)]
89. Chen, C.-L.; Hsu, Y.-C.; Yang, L.-Y.; Tung, Y.-H.; Luo, W.-B.; Liu, C.-M.; Hwang, T.-J.; Hwu, H.-G.; Tseng, W.-Y.I. Generalization of diffusion magnetic resonance imaging-based brain age prediction model through transfer learning. *NeuroImage* **2020**, *217*, 116831. [[CrossRef](#)]

90. Clements, R.G.; Claros-Olivares, C.C.; McIlvain, G.; Brockmeier, A.J.; Johnson, C.L. Mechanical Property Based Brain Age Prediction using Convolutional Neural Networks. *bioRxiv* **2023**, *13*, 2023.2002.2012.528186.
91. Wang, J.; Gao, Y.; Wang, F.; Zeng, S.; Li, J.; Miao, H.; Wang, T.; Zeng, J.; Baptista-Hon, D.; Monteiro, O.; et al. Accurate estimation of biological age and its application in disease prediction using a multimodal image Transformer system. *Proc. Natl. Acad. Sci. USA* **2024**, *121*, e2308812120. [[CrossRef](#)] [[PubMed](#)]
92. Zhou, P.; Lu, C.; Feng, J.; Lin, Z.; Yan, S. Tensor Low-Rank Representation for Data Recovery and Clustering. *IEEE Trans. Pattern Anal. Mach. Intell.* **2021**, *43*, 1718–1732. [[CrossRef](#)]
93. Wan, X.; Wang, Y.; Wang, Z.; Tang, Y.; Liu, B. Joint low-rank tensor fusion and cross-modal attention for multimodal physiological signals based emotion recognition. *Physiol. Meas.* **2024**, *45*, 075003. [[CrossRef](#)] [[PubMed](#)]
94. Gao, J.; Li, P.; Chen, Z.; Zhang, J. A survey on deep learning for multimodal data fusion. *Neural. Comput.* **2020**, *32*, 829–864. [[CrossRef](#)]
95. Li, W.; Peng, Y.; Zhang, M.; Ding, L.; Hu, H.; Shen, L. Deep model fusion: A survey. *arXiv* **2023**, arXiv:2309.15698.

**Disclaimer/Publisher’s Note:** The statements, opinions and data contained in all publications are solely those of the individual author(s) and contributor(s) and not of MDPI and/or the editor(s). MDPI and/or the editor(s) disclaim responsibility for any injury to people or property resulting from any ideas, methods, instructions or products referred to in the content.